2-Arachidonoylglycerol mobilization following brief synaptic stimulation in the dorsal lateral striatum requires glutamatergic and cholinergic neurotransmission

Daniel J. Liput[1,2], Henry L. Puhl[1], Ao Dong[3-5], Kaikai He[3,4], Yulong Li[3-6], David M. Lovinger[2]

[1]Laboratory of Molecular Physiology and [2]Laboratory for Integrative Neuroscience, National Institute on Alcohol Abuse and Alcoholism, National Institutes of Health, Maryland, USA
[3]State Key Laboratory of Membrane Biology, Peking University School of Life Sciences, Beijing, China.
[4]PKU-IDG/McGovern Institute for Brain Research, Beijing, China.
[5]Peking-Tsinghua Center for Life Sciences, Beijing, China.
[6]Chinese Institute for Brain Research, Beijing, China

Abstract

Several forms of endocannabinoid (eCB) signaling have been described in the dorsal lateral striatum (DLS), however most experimental protocols used to induce plasticity do not recapitulate the firing patterns of striatal-projecting pyramidal neurons in the cortex or firing patterns of striatal medium spiny neurons. Therefore, it is unclear if current models of eCB signaling in the DLS provide a reliable description of mechanisms engaged under physiological conditions. To address this uncertainty, we investigated mechanisms of eCB mobilization following brief synaptic stimulation that mimics *in vivo* patterns of neural activity in the DLS. To monitor eCB mobilization, the novel genetically encoded fluorescent eCB biosensor, $GRAB_{eCB2.0}$, was expressed in corticostriatal afferents of C57BL6J mice and evoked eCB transients were measured in the DLS using a brain slice photometry technique. We found that brief bouts of synaptic stimulation induce long lasting eCB transients. Inhibition of monoacylglycerol lipase, prolonged the duration of the eCB transient, while inhibition of diacylglycerol lipase inhibited the peak amplitude, suggesting that 2-AG is the predominate eCB generated following brief synaptic stimulation. 2-AG transients were robustly inhibited by AMPA and NMDA receptor antagonists, DNQX and DL-AP5 respectively. Additionally, the 2-

AG transient was inhibited by the muscarinic M1 receptor (M1R) antagonist, VU 0255035, and augmented by the M1R positive allosteric modulator, VU 0486846, indicating that acetylcholine (ACh) release is required for efficient 2-AG production. The dopamine D2 receptor (D2R) agonist, quinpirole, inhibited the 2-AG transient. However, in slices from mice lacking D2Rs on cholinergic interneurons (CINs), quinpirole did not inhibit the 2-AG transient, demonstrating that D2Rs on CINs can modulate 2-AG production. The AMPA receptor or NMDA receptor antagonists, DNQX or DL-AP5 respectively, occluded 2-AG augmentation by VU 0486846 suggesting that converging glutamatergic and cholinergic signals are required for efficient 2-AG production following brief synaptic stimulation. Collectively, these data uncover unrecognized mechanisms underlying 2-AG mobilization in the DLS.

Introduction

The endocannabinoids (eCBs) are lipid-derived signaling molecules that play a major role in synaptic modulation in the central nervous system (CNS). Unlike traditional neurotransmitters that are released from presynaptic vesicles, the eCBs are produced via enzymatic catalysis of arachidonate-containing precursor phospholipids in the plasma membrane (Ueda et al., 2013) and subsequently released from cells via a non-vesicular mechanism (Wilson and Nicoll, 2001). In the most common scenario, lipid metabolism occurs in the postsynaptic membrane and the eCBs traverse the synaptic cleft to stimulate CB1 receptors (CB1R) on presynaptic terminals, leading to inhibition of neurotransmitter release (Kano, 2014; Kreitzer and Regehr, 2001; Lovinger, 2008;

Ohno-Shosaku et al., 2001; Wilson and Nicoll, 2001). The predominant mobilization mechanism for the two main eCBs, 2-arachidonoylglycerol (2-AG) and arachidonoylethanolamide (Anandamide, AEA), is production and release “on demand” in response to membrane depolarization and subsequent Ca^{2+} influx, and/or activation of $G\alpha_{q/11}$ by g-protein coupled receptors (GPCRs). Indeed, these biochemical mechanisms underlie several forms of eCB-dependent synaptic modulation including short-term depression (STD) and long-term depression (LTD) at glutamatergic and GABAergic synapses. However, there is also evidence for tonic eCB production and signaling (Lee et al., 2010; Lee et al., 2015; Neu et al., 2007; Wilson and Nicoll, 2001).

The kinetics of eCB signaling have not been measured directly on time scales supporting synaptic modulation, but estimates have been proposed based on the onset and decay of eCB-dependent STD (Heinbockel et al., 2005). This measure involves not only the kinetics of extracellular eCB increases, but also the timing of receptor activation and presynaptic effector changes. Furthermore, although these estimates may be accurate for depolarization-induced suppression of inhibition (DSI) and other types of STD, the timing and magnitude of eCB signaling may not be universal for all forms of eCB-dependent plasticity and may not be the same for 2-AG and AEA. Additionally, the kinetics of eCB signaling and the physiological consequences do not always correlate. For example, LTD at corticostriatal and hippocampal synapses lasts for more than an hour but becomes resistant to CB1R antagonists minutes after induction (Chevaleyre and Castillo, 2003; Ronesi et al., 2004; Yin et al., 2006). Therefore, strategies other

than measuring plasticity kinetics are required to accurately measure eCB mobilization underlying physiological phenomena of interest.

CB1Rs and the appropriate eCB synthesis and degradation enzymes are abundantly expressed in the dorsal lateral striatum (DLS), and indeed multiple forms of eCB-dependent depression have been described in this brain region (Calabresi et al., 2007; Mathur and Lovinger, 2012). Perhaps the most well characterized form, LTD at corticostriatal synapses, can be induced by either high frequency stimulation (HFS)(Calabresi et al., 1992; Gerdeman et al., 2002) or low frequency stimulation (LFS)(Ronesi and Lovinger, 2005). Interestingly, these two stimulation protocols may induce LTD by differentially mobilizing AEA or 2-AG, suggesting that different modes of eCB signaling can be engaged depending on the amount of neural activity (Lerner and Kreitzer, 2012). Although HFS or long bouts of LFS result in eCB-LTD in the DLS, these stimulation patterns do not accurately recapitulate the *in vivo* firing patterns of striatal-projecting pyramidal neurons in the cortex or firing patterns of medium spiny neurons (MSNs) in the striatum (Costa et al., 2004). In other brain regions, eCB-dependent plasticity can be induced by brief bouts of synaptic stimulation (Brown et al., 2003; Galante and Diana, 2004; Maejima et al., 2001; Maejima et al., 2005), and eCBs should also be mobilized by physiologic patterns of afferent stimulation in the DLS.

Optical techniques are rapidly emerging for the study of neuromodulation in *ex vivo* and *in vivo* models. In particular, intensity-based genetically encoded biosensors, based on the GPCR scaffold, are being implemented to uncover unrecognized physiological mechanisms across multiple neurotransmitter systems (Liang et al., 2015;

Mizuno et al., 2019; Ravotto et al., 2020; Wang et al., 2018). These new generation sensors have several desirable characteristics including; inherent ligand specificity and affinity, rapid reporting dynamics, high spatial resolution, cellular targeting capability, and disabled effector coupling. A novel biosensor engineered on the GPCR platform, called $GRAB_{eCB2.0}$ (GPCR-Activation Based), was recently developed for detection of eCBs (Dong et al., 2020). This sensor was engineered by inserting a circular permutated GFP into the third intracellular loop of human CB1R and can thus report on both 2-AG and AEA signaling. We used this sensor in an *ex vivo* brain slice photometry technique to study eCB mobilization kinetics, neural activity rules supporting eCB generation, and neurochemical pathways underlying eCB synthesis and degradation in the striatum.

Materials and Methods

Animals

All animal studies were conducted in accordance with the National Institutes of Health's *Guidelines for Animal Care and Use* and all experimental protocols were approved by the National Institute on Alcohol Abuse and Alcoholism Animal Care and Use Committee. C57BL/6J and ChAT-IRES-Cre (B6.129S-$Chat^{tm1(cre)Lowl}$/MwarJ, Stock No: 031661) mice (8-10 weeks) were ordered from The Jackson Laboratory (Bar Harbor, ME, USA). $Drd2^{LoxP/LoxP}$($Drd2^{tm1Mrub}$(Bello et al., 2011)) mice were maintained in house on a C57BL/6J background. To generate mice lacking D2Rs in cholinergic interneurons, mice heterozygous for the ChAT-IRES-Cre allele and homozygous for the

Drd2LoxP allele ($Drd2^{LoxP/LoxP}ChAT^{IRES-Cre/WT}$) were bred with mice homozygous for the Drd2LoxP allele ($Drd2^{LoxP/LoxP}$). Genotypes were determined by polymerase chain reaction (PCR) using genomic DNA from ear biopsies.

Viral vectors

AAV2/9.hSyn.$GRAB_{eCB2.0}$.WPRE.hGHpolyA (Titer: $1.0x10^{13}$ GC/mL) and AAV2/9.hSyn.$GRAB_{eCBMUT}$.WPRE.hGHpolyA (Titer: $1.0x10^{13}$ GC/mL) were purchased from Vigene Biosciences (Rockville, MD, USA). AAV2/9.hSyn.$GRAB_{ACh3.0}$.WPRE.hGHpolyA (Titer: $2.4x10^{13}$ GC/mL) was packaged in house as described below. All viruses were aliquoted and stored at -80°C.

Viral production

AAV vectors were produced using a helper free triple transfection procedure similar to that previously described (Xiao et al., 1998). 293AAV cells (Cell Biolabs, Inc) were cultured in Dulbecco's modified Eagle's medium (DMEM) with GlutaMAX (ThermoFisher, Waltham, MA, USA) and supplemented with non-essential amino acids (NEAA, Gibco™), 10% FBS (Gibco™) and antibiotics (100 µg/mL penicillin and µg/mL streptomycin, Gibco™). Cells were seeded at a density of ~80% in T175 tissue culture flasks and transfected with 0.165 µg pDNA/cm^2 in a 1:1:1 molar ratio of pAAV2.hSyn.$GRAB_{ACh3.0}$.WPRE.hGHpolyA shuttle vector, pR/C9 and pHelper vectors (Cell Biolabs, San Diego, CA) complexed to polyethylenimine (PEI) (N/P ratio = 5). After 72 hr cells were harvested, resuspended in FBS-free DMEM and lysed by repeated

freeze/thaw cycles. The lysate was centrifuged at 10,000g for 20 min and the cleared supernatant was collected and incubated with benzonase (50U/mL, Sigma-Aldrich, St Louis, MO, USA) for 1 hr at 37°C. The cleared supernatant was then subject to ultracentrifugation through an iodixanol density gradient similar to previously described techniques (Strobel et al., 2015). Iodixanol gradients were layered in 13.2 mL thin wall tubes (14 x 89 mm, Beckman Coulter, Indianapolis, IN, USA). The Iodixanol steps were layered in the following order: 1 mL 60% iodixanol, 1.8 mL 40% iodixanol, 2.2 mL 25% iodixanol, 3 mL 15% iodixanol w/ 1M NaCl. The cleared supernatant containing the AAV particles was layered on top of the gradient and centrifuged in a SW41 rotor (Beckman Coulter) at 41,000 RPM for 4.5 hr at 10°C. After ultracentrifugation, the 40% iodixanol layer containing purified AAV particles was collected and the iodixanol was exchanged for dPBS and concentrated to 100 µL. The AAV sample was passed through a 0.22 µm filter and analyzed by silver stain and quantitative PCR (qPCR).

An aliquot of purified virus was serial diluted, denatured in 1 M DDT and 1x lane marker for 5 min at 90°C, and electrophoresed on a polyacrylamide gel. Gels were stained using a Pierce™ silver stain kit according to the manufacturer's instructions (ThermoFisher) and imaged using a FluorChem E system (ProteinSimple, San Jose, CA, USA). The presence of AAV particles was confirmed by visualization of the VP1, VP2 and VP3 capsid proteins and purity by the lack of other contaminating bands.

AAV titer, defined as genome copies (GC)/mL was determined by qPCR. 1 µL of AAV sample was diluted into 16 µL H_20, 1µL DNase I and 2 µL 10x DNase buffer (New England Biolabs, Ipswich, MA, USA), and incubated for 30 min at 37°C. The DNase I

161 treated sample was serial diluted (1:5, 1:20, 1:100, 1:500 and 1:2500) and stored on ice
162 for qPCR. A standard curve, using a pAAV shuttle vector containing AAV2 ITRs,
163 ranging from $2X10^5$ to $2x10^9$ plasmid copies was constructed for calculating the AAV
164 titer. Three 5 µL replicates of each sample dilution and standard curve concentration
165 were added to 15 µL of SYBR™ Green PCR master mix (ThermoFisher) containing
166 0.67 µM FWD and REV primers targeting the AAV2 ITRs. qPCR was performed on a
167 StepOnePlus™ system (ThermoFisher) using the following protocol: 3 min at 98°C,
168 (melt at 98°C for 15 sec, anneal/extend at 60°C for 30 sec) x 39 cycles. Melt curves
169 were performed to verify a single amplification product. The C_T value was defined as the
170 cycle number at which the amplification curve reached a ΔRn (Rn – baseline, where Rn
171 is the fluorescence of the reporter dye divided by the fluorescence of a passive
172 reference dye) threshold set at 0.1. A standard curve from the AAV2 plasmid standards
173 (concentration by C_T) was plotted, fit with a line and the concentration of each AAV
174 sample dilution was determined.
175
176 *Surgery*
177 Mice were anesthetized with isoflurane and stereotaxically injected with AAV
178 vectors into motor cortex (100 nL, coordinates relative to bregma in mm: A/P: + 1.1;
179 M/L: ± 1.7; D/V: - 1.6) or DLS (300 nL, coordinates relative to bregma in mm: A/P: +
180 0.75; M/L: ± 2.5; D/V: - 3.5) at a rate of 25-50 nL/min, using a 7000 series 0.5 µL
181 Hamilton syringe (Hamilton Company, Reno, NV, USA) and Pump 11 Elite Nanomite
182 (Harvard Apparatus, Holliston, MA, USA) syringe pump. Following surgery, mice were

183 given an injection of Ketoprofen (5 mg/kg, s.c.) and postoperative care was provided for
184 at least two days and until mice regained their preoperative weight.
185
186 *Slice Photometry*
187 Mice, 4-6 weeks after viral infusion, were deeply anesthetized with isoflurane,
188 decapitated and the brains extracted and placed in ice cold sucrose cutting solution (in
189 mM): 194 sucrose, 30 NaCl, 4.5 KCl, 26 $NaHCO_3$, 1.2 NaH_2PO_4, 10 D-glucose, 1 $MgCl_2$
190 saturated with 5% CO_2/ 95% O_2. Coronal brain slices (250 µm) were prepared with a
191 Leica VT1200S Vibratome (Leica Microsystems, Buffalo Grove, IL) and slices were
192 incubated at 32°C for 40-60 min in aCSF (in mM): 124 NaCl, 4.5 KCl, 26 $NaHCO_3$, 1.2
193 NaH_2PO_4, 10 D-glucose, 1 $MgCl_2$, 2 $CaCl_2$. After incubation at 32°C, slices were held at
194 room temperature until transfer to a recording chamber.
195 Photometry recordings were acquired using a Zeiss Axioscope or Olympus BX41
196 upright epifluorescence microscope equipped with a 40x 0.8 NA water emersion
197 objective. Slices were placed in a recording chamber and superfused at ~2 mL min^{-1}
198 with aCSF warmed to 29-31°C. A twisted bipolar polyimide-coated stainless-steel
199 stimulating electrode (~200 µm tip separation) was placed in the DLS just medial to the
200 corpus callosum and slightly below the tissue surface in a region with visible
201 fluorescence. Using the 40x objective, focus was adjusted to just below the tissue
202 surface, at a similar height as the electrode tips. GRAB sensors were excited using
203 either a mercury HBO 100 lamp equipped with a Zeiss FluoArc variable intensity lamp
204 controller (Carl Zeiss Microcopy GmbH, Jena, Germany) and gated with a uniblitz

205 shutter (Vincent Associates, Rochester, NY, USA), or a 470 nm light emitting diode
206 (LED, ThorLabs, Newton, NJ, USA). The Zeiss axiovert system was equipped with a
207 Zeiss 38 HE filter set (Ex. 470/40, FT 495, Em. 525/50), and the Olympus BX41 was
208 equipped with a FITC filter set (Ex. 475/28, FT 495, Em. 520/35). Excitation power was
209 measured at the sample plane using a microscope slide photodiode power sensor
210 (ThorLabs) and was 3.8 mW for the mercury HBO lamp and < 1.0 mW for the 470 nm
211 LED. A 180 μm^2 aperture located in the light path between the microscope and
212 photomultiplier tube (PMT) was used so photons were collected from a region of interest
213 just medial to the stimulation electrode tips. Photons passing through the aperture were
214 directed to a PMT (Model D-104, Photon Technology International, Edison, NJ, USA)
215 with the cathode voltage set to 300-400 V. The PMT output was amplified (gain: 0.1
216 μA/V; time constant: 5 msec), filtered at 50 Hz and digitized at 250 Hz using a Digidata
217 1322A or a 1550B and Clampex software (Axon Instruments, Molecular Devices LLC,
218 Sunnyvale, CA, USA). For all experiments, GRAB sensor measurements were acquired
219 as discrete trials repeated every 3 minutes. For each trial, the light exposure period was
220 35-45 seconds to minimize sensor photobleaching, while capturing peak responses and
221 the majority of the decay phase (**Figure 1C**). To evoke an eCB or ACh transient, a burst
222 of electrical pulses (1.0-1.5 mA, 200-500 μs) was delivered 5 s after initiating
223 fluorophore excitation. Transients were calculated as ΔF/F by averaging the PMT
224 voltage (V) for a period of 1 s just prior to electrical stimulation (F) and then calculating
225 V/F-1 for each digitized data sample.
226
227 *Drugs*

Drugs were dissolved in DMSO or dH_2O at stock concentrations, aliquoted and stored at -20°C. Just prior to use, drugs were diluted to working concentrations in aCSF. The final concentration of DMSO was < 0.1%, a concentration that did not affect evoked eCB transients. β-cyclodextrin (3.0 mg/50 mL, MilliporeSigma, Burlington, MA, USA) was included as a carrier for AM251 and DO34 solutions. The compounds 2-AG, AEA, AM251, URB597, JZL184, (-)-Quinpirole hydrochloride, VU 0255035, (RS)-3,5-Dihyroxyphenylglycine (DHPG), 6,7-Dinitroquinoxaline-2,3-dione (DNQX) disodium salt, DL-2-Amino-5-phosphonopentanoic acid (DL-AP5), JNJ16259685 and 2-Methyl-6-(phenylethynyl)pyridine (MPEP) hydrochloride were purchased from Tocris (Minneapolis MN, USA). (±)-Sulpiride was purchased from MilliporeSigma. DO34 was purchased from Aobious (Gloucester, MA, USA). VU 0486846 was generously provided by Dr. Jeffery Conn (Vanderbilt University, Nashville, TN, USA).

Data analysis

Slice photometry raw data were collected and analyzed using the pClamp™ software suit (v9.2 and v10; Molecular Devices, San Jose, CA, USA). Photometry sweeps were exported to Microsoft Excel (v16.3; Redmond, WA, USA) to calculate normalized ΔF/F traces, peak ΔF/F values, eCB mobilization time and % baseline timecourse data. Rise $t_{1/2}$ was calculated in Graphpad Prism (v8.3; San Diego, CA, USA) by fitting the rising phase of the eCB transient with an asymmetrical logistic curve. Statistical analysis and graph rendering were performed using Graphpad Prism. Baseline normalized timecourse data were analyzed using one sample t-tests, 1-way

rmANOVAs followed by Tukey's multiple comparisons test or by 2-way rmANOVAs followed by Sidak's multiple comparisons test. For t-tests and 1-way rmANOVA analysis, baseline was the average peak ΔF/F of 5 predrug sweeps (for 1-way ANOVA only), drug condition was the average peak ΔF/F of the last two data points of the drug application period (except for (RS)-DHPG experiments where only the sweep with the highest peak ΔF/F was used) and washout/antagonist wash (for 1-way ANOVA only) was the average of the last two data points during that period. Data are plotted as mean ± standard error of the mean.

Results

The novel genetically encoded biosensor, GRAB$_{eCB2.0}$, detects eCB transients induced by electrical stimulation in the DLS.

To study eCB mobilization in the DLS, we used an *ex vivo* brain slice photometry technique similar to published reports using GCaMP calcium sensors (Kupferschmidt and Lovinger, 2015; Sgobio et al., 2014). AAV2/9.hSyn.GRAB$_{eCB2.0}$ and AAV2/9.hSyn.GRABe$_{CBMUT}$ vectors were infused into motor cortex (M1/M2) of wildtype C57BL/6J mice and ~ 4-6 weeks later, eCB transients were measured at corticostriatal afferents in the DLS (**Figure 1A-C**).

Fluorescent transients from GRAB$_{eCB2.0}$ were evoked by 1s train stimulation and the amplitude of these transients increased with higher stimulation frequencies up to 100 Hz (n = 3, **Figure 1D**). To confirm the specificity of the fluorescent transients, slices were preincubated in AM251 (10 μM) for ~1 hr before performing photometry

experiments. In these slices, fluorescent transients were not detected in response to train stimulation up to 100Hz (n = 3). Additionally, evoked eCB transients could not be measured with the $GRAB_{eCBMUT}$ sensor (n = 6, **Figure 1E**), which contains the mutation F177A that greatly reduces 2-AG and AEA affinity, demonstrating that the fluorescent transients measured with $GRAB_{eCB2.0}$ are dependent on agonist occupancy of the orthosteric binding site of CB1R contained within the sensor.

In the cerebellum, brief stimulation of parallel fibers (i.e. 5 or 10 pulses at 50 Hz) triggers eCB mobilization and short-term depression (Brown et al., 2003; Maejima et al., 2001). We tested whether similar stimulation protocols are sufficient to activate eCB production in the DLS. Indeed, eCB transients could be measured in response to brief trains of electrical stimulation (**Figure 2**). Paired-pulse stimulation evoked small, but measurable, eCB transients that increased slightly in amplitude at higher frequencies. Trains of 5 or 10 pulses evoked larger transients that were augmented by increasing the stimulation frequency up to 100 Hz (**Figure 2A&B**). The eCB transients developed over several seconds measured from the start of train stimulation, with a mean $t_{1/2}$ rise time of 1.4 $\pm$ 0.03 seconds regardless of stimulation frequency (**Figure 2C**). The eCB decay phase was well described by a single exponential function and was similar across all stimulation pulse numbers and frequencies with a mean tau of 13.7 $\pm$ 0.3 seconds (**Figure 2D**).

There was a notable delay between the start of synaptic stimulation and any measurable increase in $GRAB_{eCB2.0}$ fluorescence, which we refer to as the eCB mobilization time or t_{eCB} (**Figures 2E,F**). The t_{eCB} represents the cumulative time from

294 the start of synaptic stimulation and recruitment of postsynaptic eCB production
295 machinery, to retrograde eCB transit and binding to the $GRAB_{eCB2.0}$ sensor. Thus, this
296 measurement may correlate with the minimum time required for eCB-dependent
297 presynaptic inhibition (Heinbockel et al., 2005). The t_{eCB} was measured from the start of
298 train stimulation to the time at which the presynaptic $GRAB_{eCB2.0}$ fluorescence reached a
299 threshold set at 3x rms of the baseline fluorescence and was 0.301 ± 0.01 seconds
300 regardless of stimulation frequency (**Figure 2F**).
301
302 *2-AG is the predominant eCB mobilized by brief synaptic stimulation in the DLS.*
303 Previous studies have shown that both 2-AG and AEA can be generated by
304 synaptic stimulation in the striatum, but which eCB predominates depends on the
305 specific experimental induction protocol used (Lerner and Kreitzer, 2012). To investigate
306 whether 2-AG and/or AEA are mobilized by brief synaptic stimulation, we measured the
307 effect of monoacylglycerol lipase (MAGL) or fatty acid amide hydrolase (FAAH)
308 inhibition on eCB transients evoked by a 5 pulse burst at 20Hz (**Figure 3**). Over the
309 course of 75 minutes, JZL184 (2 μM) prolonged the eCB transient decay rate (321 ±
310 69.9% of baseline, $p < 0.05$, $n = 5$), consistent with inhibition of 2-AG degradation.
311 Additionally, the basal fluorescence, F, increased (155.3 ± 21.8% of baseline, $n = 6$),
312 indicating that MAGL inhibition generates a 2-AG tone in the DLS. In contrast, bath
313 application of URB597 (1 μM) did not significantly prolong the decay rate of the evoked
314 eCB transient (**Figure 3B,** 134.6 ± 14.8% of baseline, $p > 0.05$, $n = 5$), or change the
315 basal fluorescence (108.1 ± 4.4% of baseline, $p > 0.05$, $n = 5$). To confirm that the eCB

316 transients evoked by brief synaptic stimulation were 2-AG, we tested whether
317 diacylglycerol lipase (DAGL) inhibition would inhibit the transients evoked by 5 pulse
318 bursts at 20 Hz (**Figure 3C**). Indeed, preincubating slices in the DAGL inhibitor, DO34
319 (1μM), for ~1 hr significantly reduced the peak amplitude of the eCB transient over a
320 range of stimulation intensities ($p < 0.0001$, n = 5/6).
321
322 *Metabotropic and ionotropic glutamate receptors contribute to 2-AG mobilization*
323 *following brief synaptic stimulation*
324 Group I mGluRs induce eCB-dependent plasticity at many synapses in the brain,
325 including the corticostriatal synapse (Calabresi et al., 1992; Gubellini et al., 2001;
326 Kreitzer and Malenka, 2005; Sung et al., 2001). In the DLS, mGlu1 and mGlu5 are
327 implicated in HFS-LTD and exogenous activation mGlu1/5 induces eCB-LTD (Kreitzer
328 and Malenka, 2005). Therefore, we tested whether 2-AG production evoked by brief
329 synaptic stimulation (5p 20Hz) involved recruitment of mGlu5 and/or mGlu1 (**Figure 4**).
330 Bath application of the mGlu5 negative allosteric modulator (NAM) MPEP (10 μM)
331 reduced the amplitude of the 2-AG transient to 79.8 ± 6.0% of baseline (**Figure 4A,** $p <$
332 0.01, n= 5) and bath application of the mGlu1 NAM, JNJ16259685 (JNJ'685, 1μM),
333 reduced the amplitude of the 2-AG transient to 83.9 ± 6.1% of baseline (**Figure 4B**, $p <$
334 0.05, n = 5). Given the role of mGlu5 and mGlu1 in evoked 2-AG transients, we tested
335 whether activation of mGlu1/5 with an exogenous agonist could enhance the 2-AG
336 transient. Bath application of (RS)-DHPG (100 μM) caused a biphasic change in the
337 amplitude of the evoked 2-AG transient (**Figure 4C**). The maximum augmentation was

338 173.3 ± 7.4 % of baseline, which occurred during the first evoked transient following
339 (RS)-DHPG application (n = 5, $p < 0.0001$). This modulation subsequently decayed over
340 time with the 2-AG amplitude plateauing at 75.3 ± 4.1 % of baseline (n = 5, $p < 0.05$).
341 The baseline fluorescence intensity (F, as defined in Figure 1C) was not changed by
342 (RS)-DHPG (data not shown). Collectively, these results show that group I mGluRs can
343 couple to 2-AG generation mechanisms as previously demonstrated in the DLS using
344 electrophysiology approaches, and that mGlu5 and mGlu1 activation contributes to 2-
345 AG generation following brief synaptic stimulation.
346 Postsynaptic depolarization and activation of voltage gated calcium channels is
347 required for many forms of eCB dependent STD and LTD. One presumed source of
348 depolarization for synaptically-driven eCB generation is ionotropic AMPA receptors
349 (AMPARs) (Brown et al., 2003). However, few reports directly demonstrate the
350 involvement of AMPARs in eCB production because AMPAR mediated EPSC/EPSP
351 amplitude is a primary measurement for studying eCB physiology at excitatory
352 synapses. With the ability to measure eCB generation directly using $GRAB_{eCB2.0}$, we
353 tested the hypothesis that AMPARs are a primary voltage source for synaptically driven
354 2-AG production in the DLS (**Figure 4D**). Bath application of the AMPAR antagonist,
355 DNQX (10 μM), rapidly decreased the amplitude of evoked (5p 20Hz) 2-AG transients to
356 33.1 ± 8.1% of the baseline amplitude (n = 5, $p < 0.0001$), which reversed back towards
357 baseline over a 30 min washout period (81.1 ± 3.4% baseline, $p < 0.001$ compared to
358 DNXQ). We next tested if AMPAR-dependent depolarization engaged L-type calcium
359 channels leading to 2-AG generation. Bath application of the LTCC blocker, nifedipine

(10 μM), did not reduce the amplitude of the evoked 2-AG transient (data not show), suggesting another voltage sensitive calcium channel/receptor may be responsible for triggering 2-AG generation. One possibility is the NMDA receptor (NMDAR). Indeed, bath application of the NMDAR antagonist, DL-AP5 (50 μM), resulted in a rapid reduction in the evoked 2-AG transient to 25.7% of baseline (**Figure 4E**, $n = 4$, $p < 0.0001$), which reversed back towards baseline over a 30 min washout period (65.8 ± 7.9% baseline, $p < 0.05$ compared to DL-APV).

Muscarinic M1 receptors contribute to synaptically driven 2-AG mobilization

In the dorsal striatum, muscarinic M1 receptors (M1Rs) enhance eCB-dependent DSI (Narushima et al., 2007) and are required for eCB mediated spike timing-dependent plasticity (Fino et al., 2010). On the other hand, M1Rs inhibit HFS-LTD by inhibiting L-type calcium channels (Wang et al., 2006). Given these opposing roles in modulating eCB short-term and long-term plasticity, we investigated the role of M1Rs on 2-AG generation following brief synaptic stimulation (5p 20Hz). Bath application of the M1R antagonist VU 0255035 (VU'035, 1 μM) reduced the amplitude of the evoked 2-AG transient to 36.1 ± 4.3% of the baseline ($n = 3$, $p < 0.001$), which did not washout (**Figure 5A**). To further investigate the role of M1Rs on 2-AG production, we bath applied the M1R positive allosteric modulator (PAM), VU 0486846 (VU'846, 10 μM), which increased the 2-AG peak amplitude to 274.4 ± 40.6% of baseline ($n = 5$, $p < 0.01$, **Figure 5B**). The baseline fluorescence intensity (F) was not changed by VU'035 or VU'846 (data not shown), suggesting that tonic acetylcholine (ACh) release from

382 cholinergic interneurons (CINs) does not generate an eCB tone through M1R
383 stimulation.
384
385 *M1R and Group I mGluRs facilitate 2-AG production by distinct mechanisms*
386 Both M1R and AMPAR antagonists robustly inhibited (> 60%) 2-AG production,
387 suggesting these receptors converge on a common signaling mechanism. To
388 investigate this possibility, we measured the effect of the M1R PAM, VU'846, on 2-AG
389 generation while blocking AMPA receptors (**Figure 6A**). First, DNQX (10 μM) was bath
390 applied, which reduced the 2-AG transient to 34.4 ± 2.6% of baseline (n = 3, p <
391 0.0001), a similar magnitude of inhibition as observed in the previous experiment with
392 this antagonist. After the inhibitory effect of DNQX plateaued, VU'846 (10 μM) was co-
393 applied with DNQX. DNQX completely occluded the effect of VU'846 on 2-AG
394 production (p > 0.05 compared to DNQX alone), suggesting that M1Rs and AMPARs
395 share a common signaling pathway leading to 2-AG production. It is possible that
396 AMPARs located on CINs are required for driving ACh release rather than directly
397 involved in eCB production in MSNs. To test this hypothesis, we expressed the
398 genetically encoded ACh sensor, $GRAB_{ACh3.0}$ (Jing et al., 2020) in the DLS and
399 measured ACh transients evoked by train stimulation (5 pulses at 20 Hz). Bath
400 application of DNQX (10 μM), did not change the amplitude of the evoked ACh
401 transients (data not shown), demonstrating that the role of AMPA receptors in 2-AG
402 production is not related to ACh release. Another possibility is that AMPA receptors
403 depolarize the postsynaptic cell allowing NMDA receptor activation and subsequent

Ca^{2+} influx that feeds into M1R signaling mechanisms. If this hypothesis is correct, then inhibition of NMDA receptors should also occlude the effect of VU'846 on 2-AG production. Bath application of DL-AP5 (50 μM) reduced the amplitude of the 2-AG transient to 28.6% ± 2.3% of baseline ($n = 4$, $p < 0.0001$), similar to the previous experiment with this antagonist, and occluded the effect of VU'846 on 2-AG production ($p > 0.05$ compared to DL-AP5 alone, **Figure 6B**).

Given that M1R and mGlu1/5 both couple to $G\alpha_{q/11}$ heterotrimeric g-proteins, we investigated whether (RS)-DHPG enhancement of 2-AG production was also dependent of AMPAR activation. Again, bath application of DNQX (10 μM) reduced the 2-AG transient to 30.3 ± 6.8% of baseline ($n = 3$, $p < 0.01$), however co-application of DNQX did not block (RS)-DHPG enhancement of 2-AG production ($p < 0.05$ compared to DNQX, **Figure 6C**).

Dopamine D2 receptors on cholinergic interneurons inhibit 2-AG release.

Activation of dopamine D2Rs is required for the expression of HFS-LTD in the dorsal striatum. The mechanism by which D2Rs participate in HFS-LTD has been debated in the literature, however it's clear that D2Rs on cholinergic interneurons are required for inhibiting ACh release and M1R activation (Augustin et al., 2018; Wang et al., 2006). In contrast to HFS-LTD, we found that brief synaptic stimulation requires M1R activation for 2-AG generation. Thus, we hypothesized that D2Rs would inhibit, rather than promote, 2-AG generation following brief synaptic stimulation (5p 20Hz). Indeed, bath application of the D2R agonist quinpirole (1 μM), reduced the amplitude of

evoked 2-AG transient to 61.1 ± 4.2% of baseline (n = 5, $p < 0.01$, **Figure 7A**). The specificity of this action of quinpirole for D2Rs was confirmed by co-application of the D2R antagonist, sulpiride (10 μM), which reversed the effect of quinpirole and subsequently increased the amplitude of the evoke 2-AG transient to 131.4 ± 11.5% of the initial baseline amplitude ($p < 0.05$). The rebound effect of sulpiride suggests that 20 Hz electrical stimulation elicits dopamine release from midbrain dopamine (DA) fibers to limit 2-AG generation by acting on D2Rs.

Our results showing that M1R inhibition or D2R activation suppresses 2-AG generation is consistent with the hypothesis that D2Rs on CINs are the target of quinpirole and endogenously released DA. To support of this hypothesis, we expressed the ACh sensor, $GRAB_{ACh3.0}$, in the DLS to examine the effect of D2R activation of ACh release (**Figure 7B**). ACh release evoked by 5 pulse 20 Hz train stimulation was inhibited by bath application of quinpirole (1 μM, n = 4, 39.1% of baseline, $p < 0.05$), which was reversed by the addition of sulpiride (10 μM, 101.5% of baseline, $p > 0.05$ compared to baseline).

To further confirm the role of CIN D2Rs on 2-AG production, we bred D2R-flox mice with ChAT-IRES-Cre mice to conditionally knockout D2Rs from CINs (CIN-Drd2KO) and measured the effect of quinpirole and sulpiride on 2-AG production (**Figure 7C**). Qualitatively, the 2-AG transients evoked in slices from CIN-Drd2KO mice were indistinguishable from 2-AG transients evoked in slices from wildtype C57BL/6J or $D2R^{flox/flox}$ mice. The inhibitory effect of quinpirole (1 μM) on 2-AG production was lost in slices from CIN-Drd2KO mice (n=4/5 per group, $p < 0.001$ compared to $D2R^{flox/flox}$).

Additionally, sulpiride (10 μM) did not enhance 2-AG production in slices from CIN-Drd2KO mice ($p < 0.05$ compared to $D2R^{flox/flox}$). These results confirm that stimulation of D2Rs on cholinergic interneurons, by either exogenous agonist application or endogenously release DA, inhibit 2-AG generation induced by brief synaptic stimulation.

Discussion

In this report, we used the novel genetically encoded intensity-based biosensor, $GRAB_{eCB2.0}$, in combination with brain slice photometry to study eCB signaling dynamics in the DLS. This approach offers several advantages over traditional electrophysiological techniques to studying eCB physiology. For example, we were able to make direct measurements of eCB mobilization at corticostriatal afferents, the primary site of action for eCBs, and were able study eCB mobilization mechanisms without perturbing the postsynaptic neurons. In addition, we examine the roles of ionotropic receptors more thoroughly than in past studies that relied on the function of these receptors as the readout for eCB actions. Using this approach, we show that brief bouts of synaptic stimulation induce long lasting 2-AG transients, which are dependent on convergent signals from AMPARs and $G\alpha_{q/11}$ coupled GPCRs (**Figure 8**). Our data indicate that mGlu1/5 and M1Rs trigger 2-AG mobilization though distinct mechanisms with divergent dependence on AMPAR activation and subsequent rises in intracellular Ca^{2+} concentration through NMDARs. Furthermore, D2Rs located on CINs inhibit evoked 2-AG transients by limiting ACh release and M1R stimulation. Collectively, the

present study provides new insights on circuit and cellular mechanisms controlling 2-AG mobilization in the DLS.

We measured eCB mobilization kinetics following brief, physiologically relevant, synaptic stimulation. eCB transients could be evoked by paired-pulse stimulation, but these transients were small and variable. Increasing the number of stimuli to 5 or 10 pulses produced progressively larger transients that were sensitive to stimulation frequency up to 100 Hz. Interestingly, this dependence on stimulus number and frequency closely parallels the stimulation dependence of eCB-mediated inhibition of presynaptic Ca^{2+} transients and STD induced by synaptic stimulation in the cerebellum (Brown et al., 2003; Maejima et al., 2001), suggesting that the neural activity rules supporting eCB mobilization may be generalized across brain regions. The synaptically-evoked eCB transients were slow compared to the signaling dynamics of many other neurotransmitter systems. The transients took several seconds to reach peak amplitudes and decayed over the course of tens of seconds; kinetics consistent with reported durations of eCB-dependent STD. In contrast, transients evoked by single or multiple stimuli and measured with GPCR-based ACh and DA sensors peak within less than a second and persist for only a few seconds after stimulus cessation (Jing et al., 2020; Patriarchi et al., 2018; Sun et al., 2018). The minimum time from the onset of synaptic stimulation to detecting eCBs at corticostriatal afferents, which we have defined as the eCB mobilization time (t_{eCB}), was ~300 ms regardless of stimulation protocol. In our experiments, t_{eCB} represents the cumulative time for glutamate and ACh release, post synaptic eCB generation, retrograde transit to corticostriatal membranes,

and finally activation of $GRAB_{eCB2.0}$. Thus, this measurement likely indicates the minimum time required for eCB-dependent presynaptic inhibition following synaptic stimulation. Consistent with this notion, our measurements of t_{eCB} are similar to estimates of the minimum time required for DSI expression (t_{DSI}) in CA1 pyramidal cells (Heinbockel et al., 2005).

eCB transients evoked by brief synaptic stimulation (5p 20 Hz) were sensitive to MAGL inhibition, indicating that 2-AG is mobilized under these conditions. Specifically, when $GRAB_{eCB2.0}$ was expressed in corticostriatal afferents, MAGL inhibition prolonged the decay component of the eCB transient and increased basal fluorescence, consistent with the generation of a 2-AG tone. Furthermore, DAGL inhibition decreased the peak amplitude of the of eCB transient by 75-80%, suggesting that 2-AG is the primary eCB evoked by our stimulation protocol. On the other hand, FAAH inhibition, did not significantly affect on eCB transients evoked using the same stimulation protocol, suggesting that AEA is not efficiently mobilized under these conditions.

2-AG transients evoked by brief synaptic stimulation were dependent on ionotropic and metabotropic glutamate receptors. Inhibition of mGlu5 or mGlu1 decreased the 2-AG transient by 15-20%,. Furthermore, the mGlu1/5 agonist, DHPG, increased the 2-AG transient by 175%, indicating that the 5p 20Hz train stimulation protocol does not saturate mGlu1/5 dependent eCB mobilization pathways. Interestingly, the effect of DHPG was bi-phasic as the initial potentiation of 2-AG generation gradually declined and eventually lead to depression. There are two explanations for these results. First, DHPG enhancement of 2-AG signaling may

activate a negative feedback mechanism by which the enhanced 2-AG production leads to depression of corticostriatal transmission and disengagement of AMPAR activation, which our data show is a critical component of 2-AG generation. Alternatively, it is possible that prolonged application of DHPG leads to receptor desensitization effectively reducing mGluR signaling. Supporting this mechanism, the delayed DHPG depression of 2-AG production was similar in magnitude to the inhibition observed with mGluR antagonism. We favor this latter mechanism because VU'846, an M1R PAM that also augments evoked 2-AG mobilization, did not have the same biphasic effect. However, we cannot rule out potential differences between mGluR and M1R signaling that may contribute to differences in eCB production.

We found that blocking AMPA receptors decreased the 2-AG transient by 67% indicating that these receptors are indispensable for robust 2-AG generation evoked by brief synaptic stimulation. A previous study was able to show the involvement of AMPARs in synaptically generated eCB-STD in the cerebellum by optical measurements of presynaptic Ca^{2+} transients, however, AMPARs were only a minor component (Brown et al., 2003). Our experiments suggest that AMPAR activation depolarizes the postsynaptic membrane allowing NMDAR activation and a subsequent rise in intracellular Ca^{2+}, as inhibition of NMDARs decreased the 2-AG transient by 74%.

Muscarinic M1Rs modulate STD and LTD in several brain regions. In the DLS, M1Rs are required for LTD induced by STDP protocols (Fino et al., 2010), but suppress LTD induced by HFS (Wang et al., 2006). Furthermore, M1Rs enhance DSI in MSNs and can promote DSE through synergistic actions with mGlu5 (Narushima et al., 2007;

535 Uchigashima et al., 2007). Thus, depending on the eCB induction protocol, M1Rs can
536 either promote or suppress eCB-dependent plasticity. In the current study, 2-AG
537 transients were robustly inhibited by M1R antagonists and augmented by a M1R PAM,
538 indicating that ACh released from CINs provides a major contribution to 2-AG
539 production induced by brief trains of synaptic stimulation. Our data show that blocking
540 M1Rs, AMPARs or NMDARs inhibited the eCB transient by 60-75%, suggesting these
541 receptors converge on a common signaling pathway leading to eCB production. Indeed,
542 inhibiting AMPARs or NMDARs blocked 2-AG enhancement by the M1R PAM. Our data
543 showing that AMPAR antagonists don't inhibit evoked ACh release, measured with
544 $GRAB_{ACh3.0}$, argue against a role for ionotropic glutamate receptors on CINs in the ACh
545 release that drives M1R activation. Alternatively, activation of AMPARs and NMDARs
546 on MSNs can lead to rises in intracellular Ca^{2+} that may converge with $G\alpha_{q/11}$ signaling
547 mechanisms, leading to 2-AG generation.
548 In contrast to M1Rs, the effect of mGlu1/5 stimulation is independent of AMPAR
549 activation as DHPG still enhanced the eCB transient in the presence of AMPAR
550 antagonists. These results suggest that in the context of brief synaptic stimulation,
551 M1Rs generate 2-AG though a Ca^{2+}-assisted receptor-driven eCB release (Ca^{2+}-
552 assisted RER) mechanism, while mGlu1/5s may signal by a Ca^{2+} independent
553 receptor-driven eCB release (RER) mechanism. Our findings suggesting that mGlu1/5
554 signals though an RER mechanism is consistent with reports in the hippocampus and
555 cerebellum (Chevaleyre and Castillo, 2003; Kim et al., 2002; Maejima et al., 2001). In
556 the DLS, however, DHPG-induced LTD is dependent on postsynaptic depolarization

and L-type calcium channels (Kreitzer and Malenka, 2005). Although these results are in contrast to our observations, in the striatum mGlu1/5 can trigger eCB-LTD through Ca^{2+}-dependent and Ca^{2+}-independent mechanisms (Lerner and Kreitzer, 2012). The study by Lerner and Kreitzer showed LTD requiring 2-AG mobilization is Ca^{2+} independent, consistent with our findings, while LTD requiring AEA mobilization is Ca^{2+} dependent. Indeed, Ca^{2+} dependent AEA mobilization underling HFS-LTD induction in the DLS is in agreement with previous reports (Ade and Lovinger, 2007; Calabresi et al., 1994; Choi and Lovinger, 1997). Thus, the Ca^{2+} dependence of mGlu1/5 induced eCB mobilization might depend on whether the cellular context favors 2-AG or AEA production.

Activation of D2Rs by exogenous application of quinpirole or by endogenous DA release suppressed the amplitude of evoked 2-AG transients. This result was somewhat surprising because D2R activation is required for eCB-dependent LTD in the DLS (Calabresi et al., 1992) and quinpirole inhibits evoked EPSCs in MSNs in a frequency and CB1R-dependent manner (Wang et al., 2012; Yin and Lovinger, 2006). In the context of HFS-LTD, D2Rs expressed on CINs promote eCB signaling by limiting ACh release and subsequent activation of M1Rs located on MSNs (Augustin et al., 2018; Wang et al., 2006), which is opposite to the mechanism uncovered in our study. These independent findings, although seemingly contradictory, suggest that M1Rs can either inhibit or augment eCB production, depending on the level of neural activity, and D2Rs regulate the magnitude of eCB modulation by M1Rs regardless of the sign. Importantly, 2-AG is the predominate eCB mobilized following brief synaptic stimulation in our study,

579 while evidence suggests that AEA is the predominate eCB underlying HFS-LTD (Ade
580 and Lovinger, 2007; Lerner and Kreitzer, 2012). Thus, it is conceivable that the D2R-
581 ACh-M1R signaling mechanism differently regulates 2-AG and AEA production. In
582 support of this hypothesis, activation of D2-like DA receptors increases AEA levels in
583 the dorsal striatum and limbic forebrain, while D2R inhibition increases 2-AG content in
584 limbic forebrain (Giuffrida et al., 1999; Patel et al., 2003). At the molecular level, M1Rs
585 couple to $G\alpha_{q/11}$ so 2-AG production may well occur through the canonical PLC and
586 DAGL pathway. On the other hand, M1Rs can inhibit LTCCs (Howe and Surmeier,
587 1995; Perez-Burgos et al., 2008), which is the mechanism responsible for suppressing
588 eCB-LTD and presumably AEA production. Interestingly, in our study, 2-AG production
589 required NMDARs, rather than LTCCs, thus different sources of Ca^{2+} influx may
590 contribute to differential regulation of eCBs by M1Rs.

591 In conclusion, we implemented the novel genetically encoded biosensor,
592 $GRAB_{eCB2.0}$, to uncover unrecognized signaling mechanisms underlying 2-AG
593 production in the DLS. We confirmed the involvement of ionotropic receptors in eCB
594 production, which has long been hypothesized, but largely intractable to traditional
595 electrophysiological techniques. In addition, we made direct measurements of eCB
596 production on physiological time scales, which has not been possible previously.
597 Undoubtably, $GRAB_{eCB2.0}$ will prove useful in future studies, *in vivo* and in reduced
598 preparations, to gain further insight into eCB signaling under physiological and
599 pathological conditions (Dong et al., 2020).
600

Author contributions

D.J.L and D.M.L designed the experiments. D.J.L performed the experiments and analyzed the data. A.D. K.H. and Y.L. provided the $GRAB_{eCB2.0}$ and $GRAB_{ACh3.0}$ sensor constructs. H.L.P contributed to sensor validation experiments. D.J.L. and D.M.L wrote the manuscript with input from the other authors.

Funding

This work was supported by the National Institutes of Health, National Institute on Alcohol Abuse and Alcoholism, Division of Intramural Clinical and Biological Research (ZIA AA000416).

Acknowledgements

We thank Guoxiang Luo for genotyping assistance. We are grateful to the NIAAA animal care staff for their excellent animal husbandry and veterinary care.

Figure legends

Figure 1. $GRAB_{eCB2.0}$ detects eCB transients in brain slice. A) AAV vectors encoding $GRAB_{eCB2.0}$ were infused into motor cortex (M1/M2) and fluorescence from corticostriatal afferents was measured in the DLS. B) Representative fluorescent micrographs of $GRAB_{eCB2.0}$ expression at the injection site in M1/M2 and in corticostriatal afferents in the DLS. C) Top: raw photometric recording labeled to indicate F and ΔF measurements, epifluorescence exposure time and timing of electrical stimulation.

623 Bottom: normalized eCB transient evoked by a train of electrical stimuli. D) $GRAB_{eCB2.0}$
624 fluorescent transients evoked by 1s train stimulation at the indicated frequency were
625 blocked by AM251 (n = 3 slices/group, 2-way RM ANOVA, Drug: $F_{(1,8)} = 113.8$, $p <$
626 0.0001; Frequency: $F_{(3,8)} = 5.9$, $p < 0.05$; Interaction: $F_{(3,8)} = 2.6$, $p > 0.05$) . E)
627 Fluorescent transients could not be detected with the $GRAB_{eCBMUT}$ control sensor.
628
629 **Figure 2.** Evoked eCB transients are modulated by stimulation frequency and duration.
630 A) Representative traces of eCB transients evoked by brief trains of synaptic
631 stimulation. B) The amplitude of the eCB transient increased as a function train pulse
632 number and stimulation frequency. C) The eCB transient rise time, defined at the time to
633 reach 50% of the transient peak amplitude, were similar across all stimulation protocols.
634 D) Decay kinetics were similar across all stimulation protocols. E) Schematic illustrating
635 the calculation of eCB mobilization time (t_{eCB}). F) The t_{eCB} was similar across all
636 stimulation protocols.
637
638 **Figure 3.** 2-AG is the main eCB mobilized by brief synaptic stimulation. A) Bath
639 application of MAGL inhibitor, JZL184, for 75 min prolonged the decay of the evoked
640 eCB transient (n = 5 slices, 1 sample t-test, $t_{(4)} = 3.164$, $p < 0.05$) and increased the
641 basal fluorescence (n = 6 slices, 1 sample t-test, $t_{(5)} = 2.535$, $p = 0.052$). B) Bath
642 application of the FAAH inhibitor, URB597, for 75 min had no effect on the decay of the
643 evoked eCB transient (n = 5 slices, 1 sample t-test, $t_{(4)} = 2.341$, $p > 0.05$) or basal
644 fluorescence (n = 5 slices, 1 sample t-test, $t_{(4)} = 1.858$, $p > 0.05$). C) The amplitude of

evoked eCB transients was reduced by preincubating slices in the DAGL inhibitor, DO34 (n = 5/6 slices, 2-way RM-ANOVA, Drug: $F_{(1,9)} = 48.31$, $p < 0.0001$; Amplitude: $F_{(6,54)} = 76.11$, $p < 0.0001$; Interaction: $F_{(6,54)} = 34.23$, $p < 0.0001$).

Figure 4. Synaptically evoked 2-AG transients are dependent on metabotropic and ionotropic glutamate receptors. A) The mGlu5 NAM, MPEP, decreased the peak amplitude of the 2-AG transient (n = 5 slices, 1-way RM ANOVA, Drug: $F_{(2,8)} = 12.14$, $p < 0.01$). B) The mGlu1 NAM, JNJ'685, decreased the peak amplitude of the 2-AG transient (n = 5 slices, 1-way RM ANOVA, Drug: $F_{(2,8)} = 5.531$, $p < 0.05$). C) The mGlu1/5 agonist, (RS)-DHPG, had a biphasic effect on 2-AG production (n = 5 slices, 1-way RM ANOVA, Drug: $F_{(2,8)} = 97.33$, $p < 0.0001$). D) The AMPAR antagonist, DNQX, decreased the peak amplitude of the 2-AG transient (n = 5 slices, 1-way RM ANOVA, Drug: $F_{(2,8)} = 56.91$, $p < 0.0001$). E) The NMDAR antagonist, DL-AP5, decreased the peak amplitude of the 2-AG transient (n = 4 slices, 1-way RM ANOVA, Drug: $F_{(2,6)} = 58.77$, $p < 0.0001$).

Figure 5. Muscarinic M1Rs are required for 2-AG generation evoked by brief synaptic stimulation. A) The M1R antagonist VU'035, decreased the peak amplitude of the 2-AG transient (n = 3 slices, 1-way RM ANOVA, Drug: $F_{(2,4)} = 242.8$, $p < 0.0001$). B) The M1R positive allosteric modulator VU'846 augmented the amplitude of the 2-AG transient (n = 5 slices, 1-way RM ANOVA, Drug: $F_{(2,8)} = 13.36$, $p < 0.01$).

667 **Figure 6.** M1Rs and mGlu1/5s trigger 2-AG mobilization through distinct mechanisms
668 that differentially require ionotropic glutamate receptors. A) Bath application of the
669 AMPAR antagonist, DNQX, blocks VU'846 augmentation 2-AG production (n = 3 slices,
670 1-way RM ANOVA, Drug: $F_{(2,4)} = 685.7$, $p < 0.0001$). B) Bath application of the NMDAR
671 antagonist, DL-AP5, blocks VU'846 augmentation 2-AG production (n = 4 slices, 1-way
672 RM ANOVA, Drug: $F_{(2,6)} = 402.3$, $p < 0.0001$). C) (RS)-DHPG transiently augments 2-
673 AG production in the presence of DNQX (n = 3 slices, 1-way RM ANOVA, Drug: $F_{(2,4)} =$
674 52.17, $p < 0.0001$).
675
676 **Figure 7.** D2Rs expressed on CINs inhibit 2-AG production. A) The D2R agonist,
677 quinpirole, decreased the peak amplitude of the evoked 2-AG transient and the D2R
678 antagonist, sulpiride, reversed the effect of quinpirole and increased the amplitude of
679 the 2-AG transient above baseline (n = 5 slices, 1-way RM ANOVA, Drug: $F_{(2,8)} = 29.59$,
680 $p < 0.001$). B) Quinpirole reduced evoked ACh release, as measured with $GRAB_{ACh3.0}$,
681 which was reversed by sulpiride (n = 4 slices, 1-way RM ANOVA, Drug: $F_{(2,6)} = 10.99$, p
682 < 0.01). C) Conditional knockout out of D2Rs on CINs precludes the effects of quinpirole
683 and sulpiride. (n = 4/5 slices/group, 2-way RM ANOVA, Drug: $F_{(14,98)} = 10.23$, $p <$
684 0.0001; Genotype: $F_{(1,7)} = 0.7338$, $p < 0.05$; Interaction: $F_{(14,98)} = 15.14$, $p > 0.0001$).
685
686 **Figure 8.** Cartoon illustrating the circuit and cellular mechanisms underlying 2-AG
687 mobilization following brief synaptic stimulation. Our data are consistent with a model in

688 which synaptic stimulation in the DLS generates 2-AG though converging glutamatergic
689 and cholinergic neurotransmission.
690
691
692 **References**

693 Ade, K.K., and Lovinger, D.M. (2007). Anandamide regulates postnatal development of long-
694 term synaptic plasticity in the rat dorsolateral striatum. J Neurosci *27*, 2403-2409.
695 Augustin, S.M., Chancey, J.H., and Lovinger, D.M. (2018). Dual Dopaminergic Regulation of
696 Corticostriatal Plasticity by Cholinergic Interneurons and Indirect Pathway Medium Spiny
697 Neurons. Cell Rep *24*, 2883-2893.
698 Bello, E.P., Mateo, Y., Gelman, D.M., Noain, D., Shin, J.H., Low, M.J., Alvarez, V.A.,
699 Lovinger, D.M., and Rubinstein, M. (2011). Cocaine supersensitivity and enhanced motivation
700 for reward in mice lacking dopamine D2 autoreceptors. Nat Neurosci *14*, 1033-1038.
701 Brown, S.P., Brenowitz, S.D., and Regehr, W.G. (2003). Brief presynaptic bursts evoke synapse-
702 specific retrograde inhibition mediated by endogenous cannabinoids. Nat Neurosci *6*, 1048-1057.
703 Calabresi, P., Maj, R., Pisani, A., Mercuri, N.B., and Bernardi, G. (1992). Long-term synaptic
704 depression in the striatum: physiological and pharmacological characterization. J Neurosci *12*,
705 4224-4233.
706 Calabresi, P., Picconi, B., Tozzi, A., and Di Filippo, M. (2007). Dopamine-mediated regulation
707 of corticostriatal synaptic plasticity. Trends Neurosci *30*, 211-219.
708 Calabresi, P., Pisani, A., Mercuri, N.B., and Bernardi, G. (1994). Post-receptor mechanisms
709 underlying striatal long-term depression. J Neurosci *14*, 4871-4881.
710 Chevaleyre, V., and Castillo, P.E. (2003). Heterosynaptic LTD of hippocampal GABAergic
711 synapses: a novel role of endocannabinoids in regulating excitability. Neuron *38*, 461-472.
712 Choi, S., and Lovinger, D.M. (1997). Decreased probability of neurotransmitter release underlies
713 striatal long-term depression and postnatal development of corticostriatal synapses. Proc Natl
714 Acad Sci U S A *94*, 2665-2670.
715 Costa, R.M., Cohen, D., and Nicolelis, M.A. (2004). Differential corticostriatal plasticity during
716 fast and slow motor skill learning in mice. Curr Biol *14*, 1124-1134.
717 Dong, A., He, K., Dudok, B., Farrell, J.S., Guan, W., Liput, D.J., Puhl, H.L., Cai, R., Duan, J.,
718 Albarran, E.*, et al.* (2020). A fluorescent sensor for spatiotemporally resolved endocannabinoid
719 dynamics *in vitro* and *in vivo*. bioRxiv, 2020.2010.2008.329169.
720 Fino, E., Paille, V., Cui, Y., Morera-Herreras, T., Deniau, J.M., and Venance, L. (2010). Distinct
721 coincidence detectors govern the corticostriatal spike timing-dependent plasticity. J Physiol *588*,
722 3045-3062.
723 Galante, M., and Diana, M.A. (2004). Group I metabotropic glutamate receptors inhibit GABA
724 release at interneuron-Purkinje cell synapses through endocannabinoid production. J Neurosci
725 *24*, 4865-4874.
726 Gerdeman, G.L., Ronesi, J., and Lovinger, D.M. (2002). Postsynaptic endocannabinoid release is
727 critical to long-term depression in the striatum. Nat Neurosci *5*, 446-451.

Giuffrida, A., Parsons, L.H., Kerr, T.M., Rodriguez de Fonseca, F., Navarro, M., and Piomelli, D. (1999). Dopamine activation of endogenous cannabinoid signaling in dorsal striatum. Nat Neurosci *2*, 358-363.

Gubellini, P., Saulle, E., Centonze, D., Bonsi, P., Pisani, A., Bernardi, G., Conquet, F., and Calabresi, P. (2001). Selective involvement of mGlu1 receptors in corticostriatal LTD. Neuropharmacology *40*, 839-846.

Heinbockel, T., Brager, D.H., Reich, C.G., Zhao, J., Muralidharan, S., Alger, B.E., and Kao, J.P. (2005). Endocannabinoid signaling dynamics probed with optical tools. J Neurosci *25*, 9449-9459.

Howe, A.R., and Surmeier, D.J. (1995). Muscarinic receptors modulate N-, P-, and L-type Ca2+ currents in rat striatal neurons through parallel pathways. J Neurosci *15*, 458-469.

Jing, M., Li, Y., Zeng, J., Huang, P., Skirzewski, M., Kljakic, O., Peng, W., Qian, T., Tan, K., Zou, J.*, et al.* (2020). An optimized acetylcholine sensor for monitoring in vivo cholinergic activity. Nat Methods.

Kano, M. (2014). Control of synaptic function by endocannabinoid-mediated retrograde signaling. Proc Jpn Acad Ser B Phys Biol Sci *90*, 235-250.

Kim, J., Isokawa, M., Ledent, C., and Alger, B.E. (2002). Activation of muscarinic acetylcholine receptors enhances the release of endogenous cannabinoids in the hippocampus. J Neurosci *22*, 10182-10191.

Kreitzer, A.C., and Malenka, R.C. (2005). Dopamine modulation of state-dependent endocannabinoid release and long-term depression in the striatum. J Neurosci *25*, 10537-10545.

Kreitzer, A.C., and Regehr, W.G. (2001). Retrograde inhibition of presynaptic calcium influx by endogenous cannabinoids at excitatory synapses onto Purkinje cells. Neuron *29*, 717-727.

Kupferschmidt, D.A., and Lovinger, D.M. (2015). Inhibition of presynaptic calcium transients in cortical inputs to the dorsolateral striatum by metabotropic GABA(B) and mGlu2/3 receptors. J Physiol *593*, 2295-2310.

Lee, S.H., Foldy, C., and Soltesz, I. (2010). Distinct endocannabinoid control of GABA release at perisomatic and dendritic synapses in the hippocampus. J Neurosci *30*, 7993-8000.

Lee, S.H., Ledri, M., Toth, B., Marchionni, I., Henstridge, C.M., Dudok, B., Kenesei, K., Barna, L., Szabo, S.I., Renkecz, T.*, et al.* (2015). Multiple Forms of Endocannabinoid and Endovanilloid Signaling Regulate the Tonic Control of GABA Release. J Neurosci *35*, 10039-10057.

Lerner, T.N., and Kreitzer, A.C. (2012). RGS4 is required for dopaminergic control of striatal LTD and susceptibility to parkinsonian motor deficits. Neuron *73*, 347-359.

Liang, R., Broussard, G.J., and Tian, L. (2015). Imaging chemical neurotransmission with genetically encoded fluorescent sensors. ACS Chem Neurosci *6*, 84-93.

Lovinger, D.M. (2008). Presynaptic modulation by endocannabinoids. Handb Exp Pharmacol, 435-477.

Maejima, T., Hashimoto, K., Yoshida, T., Aiba, A., and Kano, M. (2001). Presynaptic inhibition caused by retrograde signal from metabotropic glutamate to cannabinoid receptors. Neuron *31*, 463-475.

Maejima, T., Oka, S., Hashimotodani, Y., Ohno-Shosaku, T., Aiba, A., Wu, D., Waku, K., Sugiura, T., and Kano, M. (2005). Synaptically driven endocannabinoid release requires Ca2+-assisted metabotropic glutamate receptor subtype 1 to phospholipase Cbeta4 signaling cascade in the cerebellum. J Neurosci *25*, 6826-6835.

773 Mathur, B.N., and Lovinger, D.M. (2012). Endocannabinoid-dopamine interactions in striatal
774 synaptic plasticity. Front Pharmacol *3*, 66.
775 Mizuno, G.O., Unger, E.K., and Tian, L. (2019). Real Time Monitoring of Neuromodulators in
776 Behaving Animals Using Genetically Encoded Indicators. In Compendium of In Vivo
777 Monitoring in Real-Time Molecular Neuroscience, pp. 1-18.
778 Narushima, M., Uchigashima, M., Fukaya, M., Matsui, M., Manabe, T., Hashimoto, K.,
779 Watanabe, M., and Kano, M. (2007). Tonic enhancement of endocannabinoid-mediated
780 retrograde suppression of inhibition by cholinergic interneuron activity in the striatum. J
781 Neurosci *27*, 496-506.
782 Neu, A., Foldy, C., and Soltesz, I. (2007). Postsynaptic origin of CB1-dependent tonic inhibition
783 of GABA release at cholecystokinin-positive basket cell to pyramidal cell synapses in the CA1
784 region of the rat hippocampus. J Physiol *578*, 233-247.
785 Ohno-Shosaku, T., Maejima, T., and Kano, M. (2001). Endogenous cannabinoids mediate
786 retrograde signals from depolarized postsynaptic neurons to presynaptic terminals. Neuron *29*,
787 729-738.
788 Patel, S., Rademacher, D.J., and Hillard, C.J. (2003). Differential regulation of the
789 endocannabinoids anandamide and 2-arachidonylglycerol within the limbic forebrain by
790 dopamine receptor activity. J Pharmacol Exp Ther *306*, 880-888.
791 Patriarchi, T., Cho, J.R., Merten, K., Howe, M.W., Marley, A., Xiong, W.H., Folk, R.W.,
792 Broussard, G.J., Liang, R., Jang, M.J.*, et al.* (2018). Ultrafast neuronal imaging of dopamine
793 dynamics with designed genetically encoded sensors. Science *360*.
794 Perez-Burgos, A., Perez-Rosello, T., Salgado, H., Flores-Barrera, E., Prieto, G.A., Figueroa, A.,
795 Galarraga, E., and Bargas, J. (2008). Muscarinic M(1) modulation of N and L types of calcium
796 channels is mediated by protein kinase C in neostriatal neurons. Neuroscience *155*, 1079-1097.
797 Ravotto, L., Duffet, L., Zhou, X., Weber, B., and Patriarchi, T. (2020). A Bright and Colorful
798 Future for G-Protein Coupled Receptor Sensors. Front Cell Neurosci *14*, 67.
799 Ronesi, J., Gerdeman, G.L., and Lovinger, D.M. (2004). Disruption of endocannabinoid release
800 and striatal long-term depression by postsynaptic blockade of endocannabinoid membrane
801 transport. J Neurosci *24*, 1673-1679.
802 Ronesi, J., and Lovinger, D.M. (2005). Induction of striatal long-term synaptic depression by
803 moderate frequency activation of cortical afferents in rat. J Physiol *562*, 245-256.
804 Sgobio, C., Kupferschmidt, D.A., Cui, G., Sun, L., Li, Z., Cai, H., and Lovinger, D.M. (2014).
805 Optogenetic measurement of presynaptic calcium transients using conditional genetically
806 encoded calcium indicator expression in dopaminergic neurons. PLoS One *9*, e111749.
807 Strobel, B., Miller, F.D., Rist, W., and Lamla, T. (2015). Comparative Analysis of Cesium
808 Chloride- and Iodixanol-Based Purification of Recombinant Adeno-Associated Viral Vectors for
809 Preclinical Applications. Hum Gene Ther Methods *26*, 147-157.
810 Sun, F., Zeng, J., Jing, M., Zhou, J., Feng, J., Owen, S.F., Luo, Y., Li, F., Wang, H., Yamaguchi,
811 T.*, et al.* (2018). A Genetically Encoded Fluorescent Sensor Enables Rapid and Specific
812 Detection of Dopamine in Flies, Fish, and Mice. Cell *174*, 481-496 e419.
813 Sung, K.W., Choi, S., and Lovinger, D.M. (2001). Activation of group I mGluRs is necessary for
814 induction of long-term depression at striatal synapses. J Neurophysiol *86*, 2405-2412.
815 Uchigashima, M., Narushima, M., Fukaya, M., Katona, I., Kano, M., and Watanabe, M. (2007).
816 Subcellular arrangement of molecules for 2-arachidonoyl-glycerol-mediated retrograde signaling
817 and its physiological contribution to synaptic modulation in the striatum. J Neurosci *27*, 3663-
818 3676.

819 Ueda, N., Tsuboi, K., and Uyama, T. (2013). Metabolism of endocannabinoids and related N-
820 acylethanolamines: canonical and alternative pathways. FEBS J *280*, 1874-1894.
821 Wang, H., Jing, M., and Li, Y. (2018). Lighting up the brain: genetically encoded fluorescent
822 sensors for imaging neurotransmitters and neuromodulators. Curr Opin Neurobiol *50*, 171-178.
823 Wang, W., Dever, D., Lowe, J., Storey, G.P., Bhansali, A., Eck, E.K., Nitulescu, I., Weimer, J.,
824 and Bamford, N.S. (2012). Regulation of prefrontal excitatory neurotransmission by dopamine in
825 the nucleus accumbens core. J Physiol *590*, 3743-3769.
826 Wang, Z., Kai, L., Day, M., Ronesi, J., Yin, H.H., Ding, J., Tkatch, T., Lovinger, D.M., and
827 Surmeier, D.J. (2006). Dopaminergic control of corticostriatal long-term synaptic depression in
828 medium spiny neurons is mediated by cholinergic interneurons. Neuron *50*, 443-452.
829 Wilson, R.I., and Nicoll, R.A. (2001). Endogenous cannabinoids mediate retrograde signalling at
830 hippocampal synapses. Nature *410*, 588-592.
831 Xiao, X., Li, J., and Samulski, R.J. (1998). Production of high-titer recombinant adeno-
832 associated virus vectors in the absence of helper adenovirus. J Virol *72*, 2224-2232.
833 Yin, H.H., Davis, M.I., Ronesi, J.A., and Lovinger, D.M. (2006). The role of protein synthesis in
834 striatal long-term depression. J Neurosci *26*, 11811-11820.
835 Yin, H.H., and Lovinger, D.M. (2006). Frequency-specific and D2 receptor-mediated inhibition
836 of glutamate release by retrograde endocannabinoid signaling. Proc Natl Acad Sci U S A *103*,
837 8251-8256.
838

Figure 1

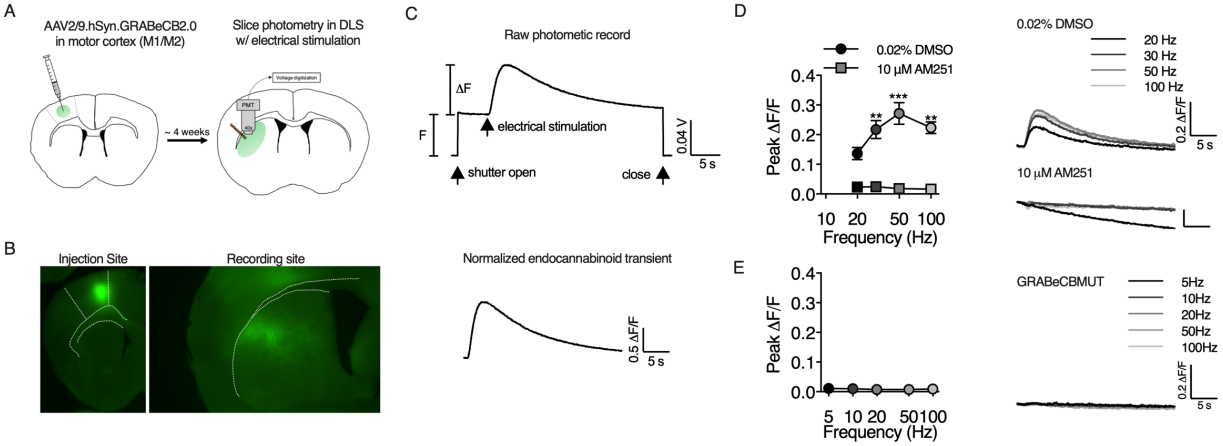

Figure 2

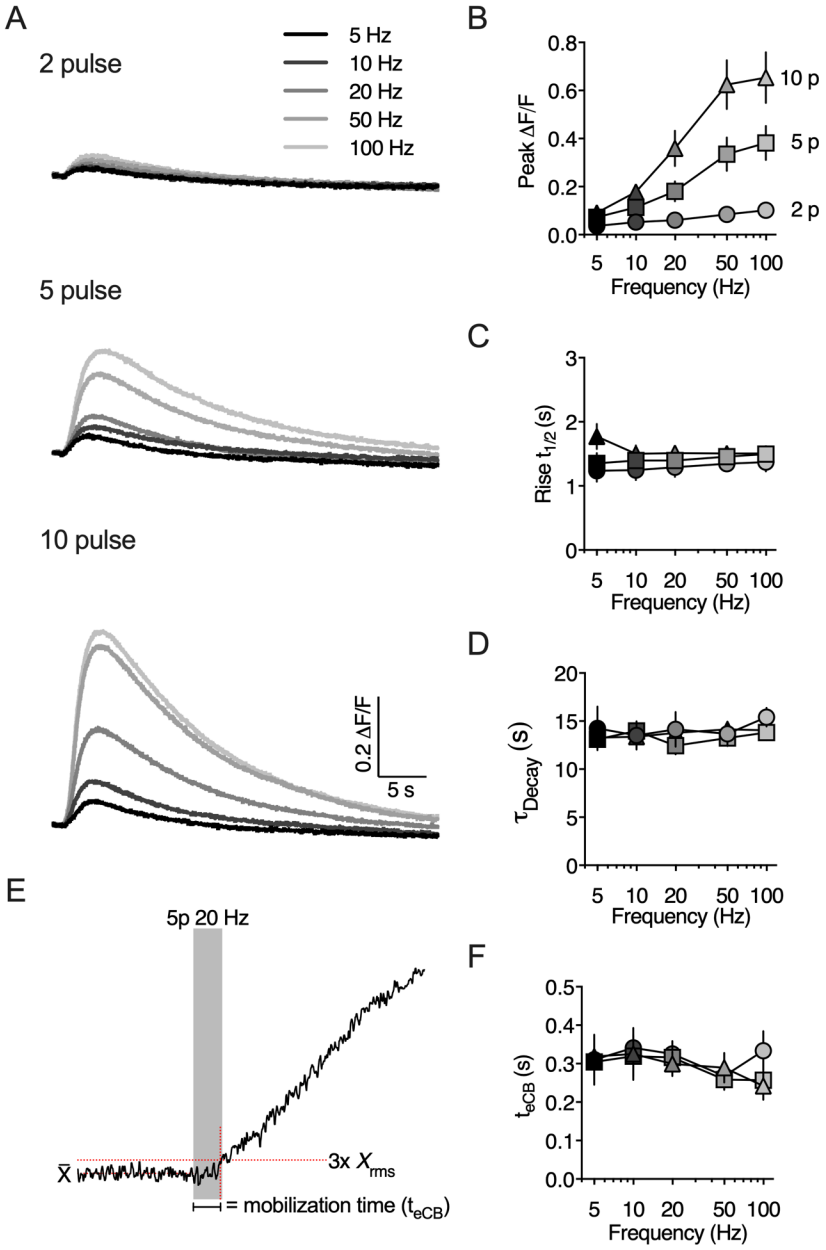

Figure 3

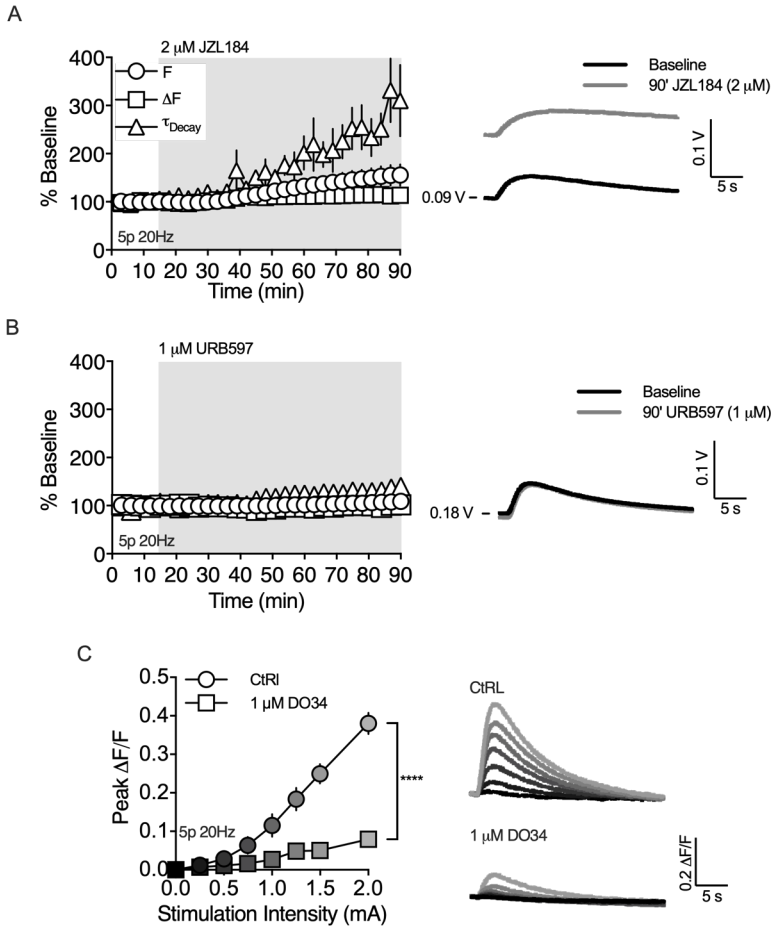

Figure 4

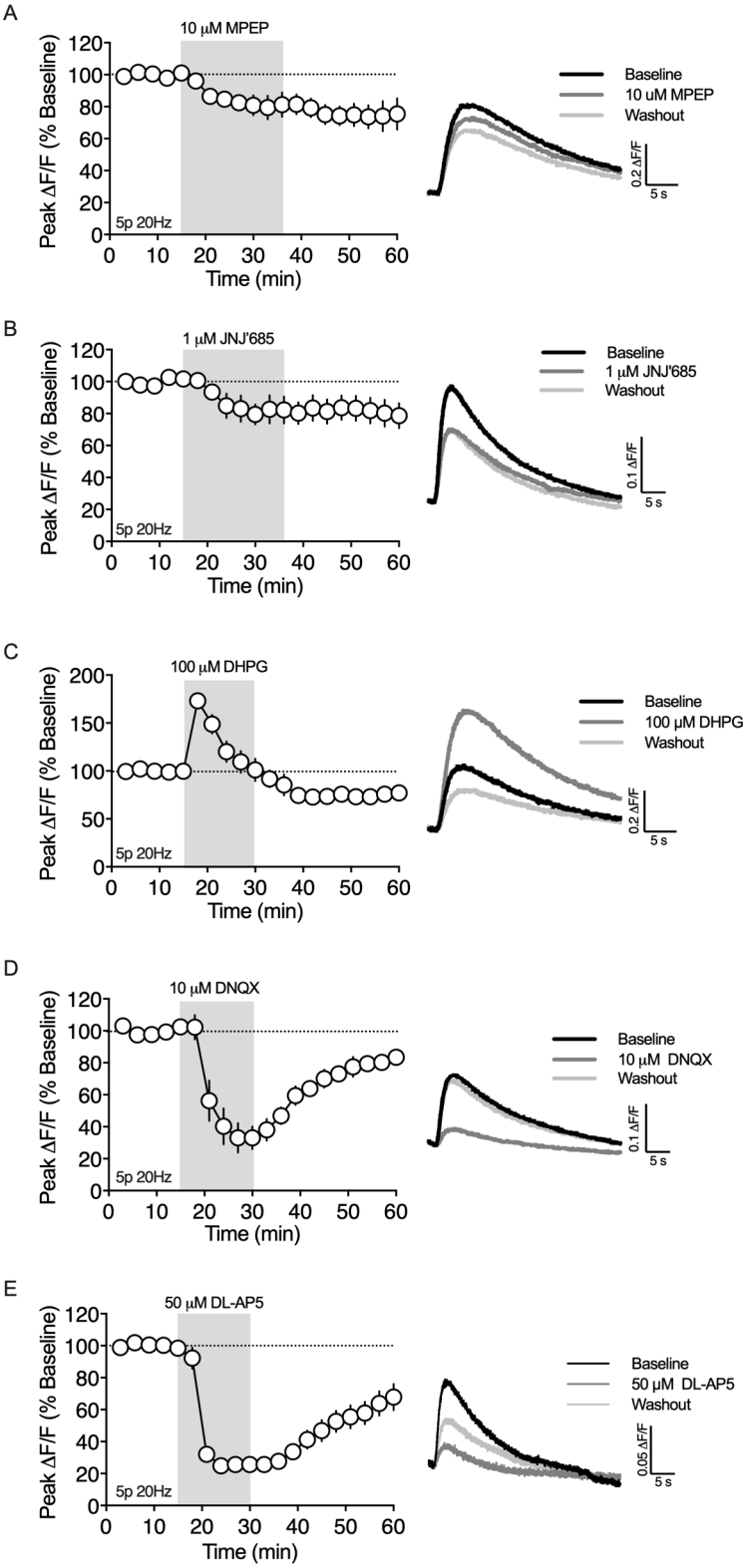

Figure 5

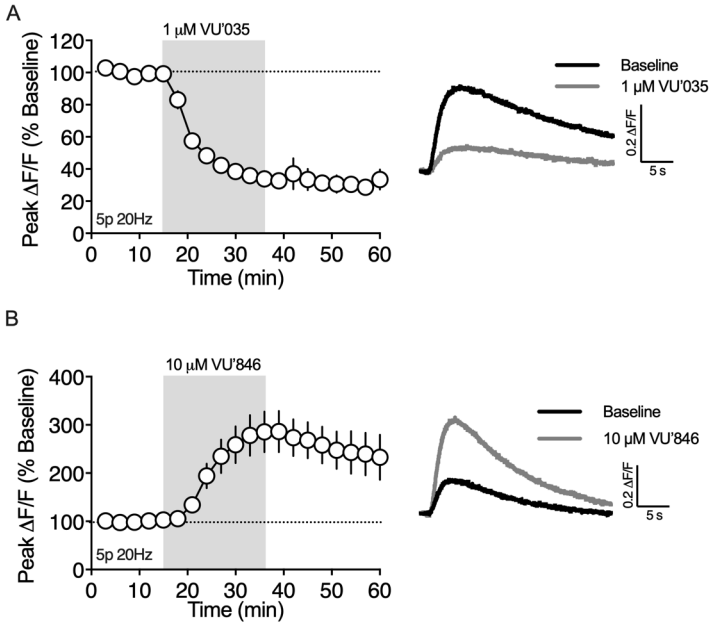

Figure 6

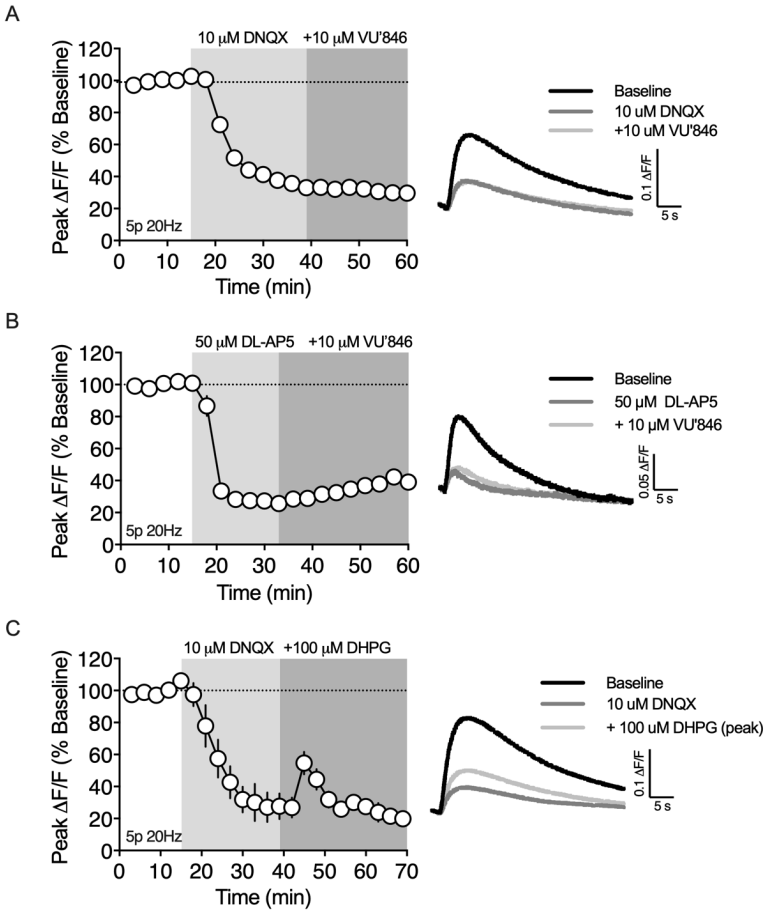

Figure 7

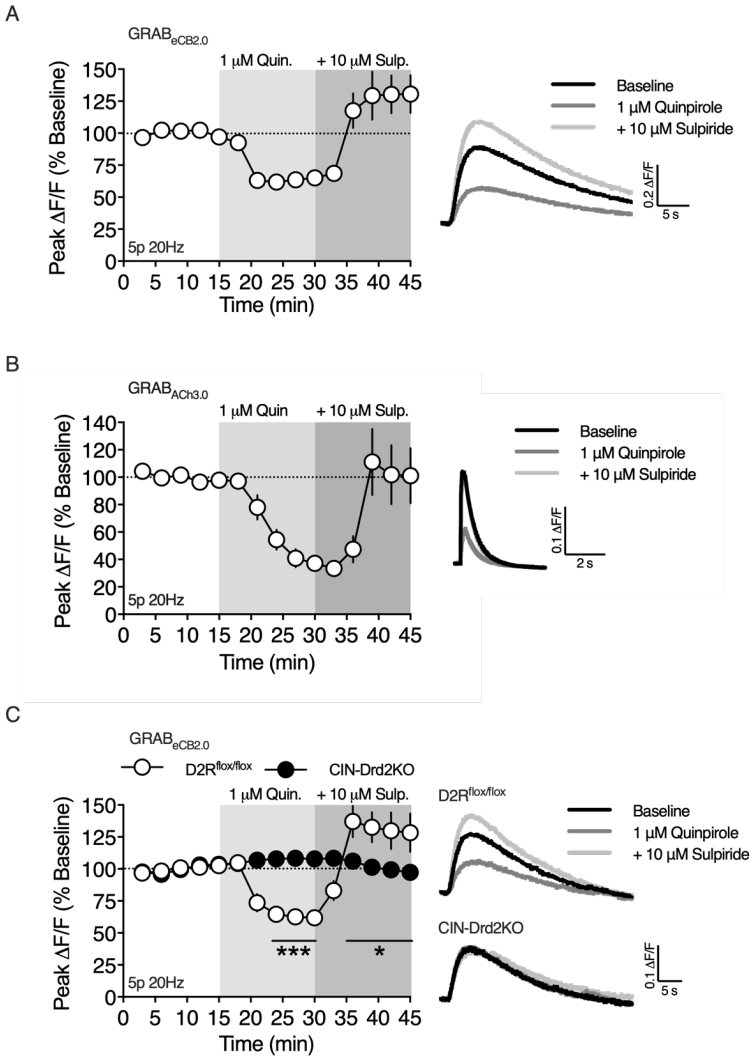

Figure 8